

Transmission properties of terahertz pulses through an ultrathin subwavelength silicon hole array

Abul K. Azad, Y. Zhao, and W. Zhang^{a)}

School of Electrical and Computer Engineering, Oklahoma State University, Stillwater, Oklahoma 74078

(Received 29 October 2004; accepted 21 February 2005; published online 30 March 2005)

We demonstrate extraordinary THz transmission of an array of subwavelength apertures patterned on ultrathin highly doped silicon by reactive ion etching. The zero-order transmission spectra exhibit well-defined maxima and minima which are attributed to the excitation of surface-plasmon polaritons and Wood's anomaly. The transmission anisotropy is investigated with respect to the orientation of the elliptical hole array in the frequency range from 0.2 to 3.5 THz, and we notice that the transmission increases significantly when the major axis of the elliptical hole is perpendicular to the polarization of THz beam. In addition, redshift and reduction in transmission amplitude are observed when the surrounding dielectric permittivity is increased. © 2005 American Institute of Physics. [DOI: 10.1063/1.1897842]

The enhanced transmission of light through the array of subwavelength holes perforated on an optically thick metallic surface discovered by Ebbesen *et al.*¹ has inspired great interest to explore the underlying physics and the possible applications of surface plasmons. Extensive theoretical and experimental studies have been carried out to explain the physical phenomena behind the enhanced transmission process, which suggests that the enhanced transmission below the cutoff frequency defined by hole size is due to the resonant excitation of surface-plasmon polaritons (SPPs).²⁻⁵ The SPPs excited on periodically structured metal by the incident light tunnel through the subwavelength holes and reradiate as light on the opposite side. The interesting properties of SPPs can localize and concentrate the electromagnetic waves in the subwavelength scale which lead to the potential applications in developing integrated photonic devices.^{5,6} At THz frequencies, the surface-plasmon-enhanced transmission through the thin subwavelength metallic hole arrays has been reported recently.^{7,8} The experimental results showed that the hole shape had a significant effect on the THz transmission magnitude, whereas in the optical region hole shape was not a crucial parameter for the transmission coefficient.⁹ THz SPPs were also excited at an interface between a thin dielectric film and metal surface, demonstrating the potential applications of SPPs in biosensing.¹⁰

In the THz region, it has been demonstrated that highly doped semiconductors show metallic behavior because the real part of the permittivity possesses a negative value which supports the formation of surface plasmons.¹¹ The enhanced THz transmission was also observed in a microstructured hole array in highly doped silicon where the extraordinary transmission was attributed to the tunneling via excitation of the resonant SPPs through the subwavelength structures. Transmission amplitude has also been studied as a function of the size of the square hole arrays and the thickness of the grating.¹² The trend of the experimental results indicated that the transmission increases nearly exponentially as the thickness of the grating is reduced.

In this letter, we present experimental results in the frequency range of 0.2–3.5 THz of SPP-enhanced transmission

of THz pulses through a subwavelength elliptical hole array of 50- μm -thick, highly doped, *n*-type silicon processed by reactive ion etching (RIE). The measured peak of the transmission magnitude by THz time-domain spectroscopy (THz-TDS) shows a 42% amplitude efficiency. The orientation-dependent THz transmission of the elliptical shaped hole array has been investigated. When the major axis of the aperture is perpendicular to the polarization of THz electric field, we observe a significant increase in the transmission magnitude. In addition, we have studied the effect of the surrounding dielectric materials on THz transmission properties. The peak transmission magnitude reduces and shifts toward lower frequency with the increasing refractive indices of the surrounding materials. This extraordinary transmission may find applications in THz optoelectronic devices, such as high throughput, high-resolution filters, and focusing elements for the THz imaging systems.

The sample used in this experiment was processed from a commercially available *n*-type 50- μm -thick silicon wafer with a resistivity of $2 \times 10^{-3} \Omega \text{ cm}$ and a corresponding high carrier concentration of $3 \times 10^{19} \text{ cm}^{-3}$. The carrier density and the thickness of the doped silicon are chosen to ensure that no THz transmission is observed through the unstructured silicon slab. In our case, the corresponding amplitude absorption length is less than 1 μm at 1 THz. The fabrication processes of the subwavelength hole array have included the conventional photolithography and RIE. The wafer was spin coated with SU-8 2025 photoresist (Microchem) and exposed with a UV light source while under the mask. After development, the RIE process has created through holes on the bare silicon while the rest of the area on the wafer was still protected by photoresist. A mixed gas flow of 12.5 sccm SF_6 and 1.5 sccm O_2 , driven under a RF power of 400 W, gave an etching rate of 5 $\mu\text{m}/\text{min}$ for silicon. Figure 1 shows the scanning electron microscope (SEM) picture of the elliptical hole array with a periodicity of 160 μm and dimensions of 75 μm along the major axis (*y*) and 45 μm along the minor axis (*x*).

The THz system used in this work is a photoconductive switch-based THz-TDS spectrometer with 4.5 THz broad bandwidth.^{7,13} In order to compress the THz beam to a diameter comparable to the size of the array sample, an addi-

^{a)}Electronic mail: wwzhang@okstate.edu

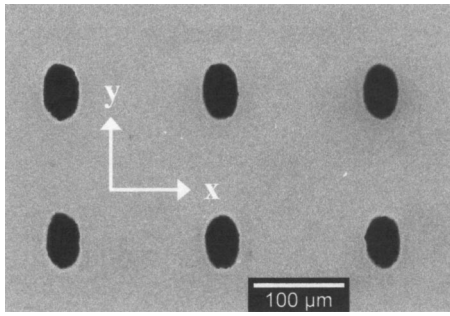


FIG. 1. SEM image of the subwavelength, elliptical hole array fabricated on a highly doped n -type, 50- μm -thick silicon wafer. The dimensions of the array are 75 μm along the major axis and 45 μm along the minor axis with a period of 160 μm in both axes.

tional pair of 50 mm paraboloidal mirrors are placed midway between the two major paraboloidal mirrors. As a result, a frequency independent 3.5-mm-diameter THz waist is obtained and on which a 5-mm-sample clear aperture is centered. The transmitted sample and reference electrical fields are recorded in the time domain, and the frequency dependent amplitude and phase information are derived from the ratio of the Fourier-transformed spectra. The transmission measurements are performed with a linearly polarized THz beam impinging on the sample at normal incidence.

For normal incidence, the resonant wavelengths for the excitation of SPPs of a rectangular lattice structure are approximately given by¹⁴

$$\lambda_{\text{sp}}^{m,n} \cong \frac{L}{\sqrt{m^2 + n^2}} \sqrt{\frac{\epsilon_1 \epsilon_2}{\epsilon_1 + \epsilon_2}}, \quad (1)$$

where ϵ_1 is the dielectric constant of the surrounding material; $\epsilon_2 = \epsilon_{r2} + i\epsilon_{i2}$ is the dielectric constant of the metal-like grating materials, for which ϵ_{r2} and ϵ_{i2} are the real and imaginary part, respectively; L is the lattice constant; and m and n are the integer mode indices. It has been experimentally demonstrated that SPP-assisted transmission increases with the higher value of the ratio between the real and imaginary part of the dielectric constant, $-\epsilon_{r2}/\epsilon_{i2}$.¹⁵ For most metals, ϵ_{r2} has negative value; at optical frequencies, the ratio $-\epsilon_{r2}/\epsilon_{i2} \gg 1$ whereas $-\epsilon_{r2}/\epsilon_{i2} < 1$ at THz frequencies. For aluminum, $-\epsilon_{r2}/\epsilon_{i2} = 5.10$ at $\lambda = 1.24 \mu\text{m}$;¹⁶ while $-\epsilon_{r2}/\epsilon_{i2} = 0.05$ at 1.0 THz ($\lambda = 300 \mu\text{m}$).⁷ However, Moreno *et al.*¹⁷ demonstrated that appropriate periodic corrugation of the two-dimensional (2D) array surface changes the effective dielectric constant which facilitates the establishment of SPPs. As a result, the enhanced transmission can be realized even with smaller ratio of $-\epsilon_{r2}/\epsilon_{i2}$ at THz frequencies. The complex dielectric constant of our silicon sample was calculated using the simple Drude model.¹⁸ With the given n -type carrier density, $3 \times 10^{19} \text{ cm}^{-3}$ and the corresponding electron mobility, 120 $\text{cm}^2/\text{V s}$,¹⁹ the real and imaginary dielectric constant are $\epsilon_{r2} = -103$, and $\epsilon_{i2} = 1020$, respectively, at 1.0 THz. The ratio $-\epsilon_{r2}/\epsilon_{i2} = 0.10$ is comparable with that in aluminum (Ref. 7) and thus is sufficient to support the excitation of SPPs in the THz spectral region.

To examine the orientation-dependent enhanced transmission, the sample was first oriented in a way that the THz polarization is perpendicular to the major axis of the elliptical hole ($E \parallel x$), then it was rotated by 90°, enabling the polarization of THz beam parallel to the major axis of the hole ($E \parallel y$). The frequency-dependent transmission amplitude

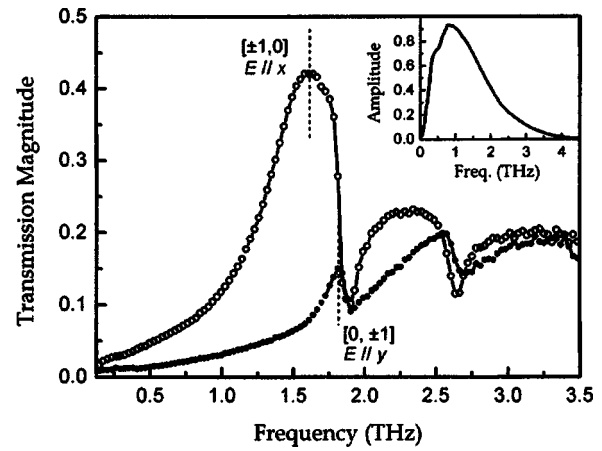


FIG. 2. Transmission amplitude spectra defined by the ratio between the spectra of the sample and the reference pulses through the array in different orientations: The major axis perpendicular to the polarization of THz beam (open circles), and the major axis parallel to the polarization of THz beam (dots). The dashed lines represent the resonance peaks. The normalized reference spectrum is plotted in the inset.

spectra for both orientations are shown in Fig. 2. The transmission is obtained from the ratio between the Fourier-transformed sample and the reference amplitudes. The inset of Fig. 2 shows the normalized reference amplitude spectrum. For the case of $E \parallel x$, the transmission spectrum shows a pronounced peak at 1.6 THz, well below the cutoff, which is 2.0 THz as determined by the 75- μm -sized holes. The peak of the transmission magnitude is due to the resonance of SPPs and can be attributed to the $[\pm 1, 0]$ surface-plasmon mode as indicated by a dashed line in Fig. 2. We observe 42% amplitude transmission for the $[\pm 1, 0]$ mode at the silicon-air interface. Compared to the prediction for the 110- μm -sized rectangular hole grating,¹² this measured amplitude efficiency shows a higher value and can be attributed to the different shape of the holes.⁷

In the $E \parallel y$ orientation, the resonance peak of the SP $[0, \pm 1]$ mode is located at 1.8 THz and shows an amplitude transmission of 16% as shown in Fig. 2. The effect of the hole structure on THz transmission has been demonstrated in Ref. 7, where a higher transmission magnitude was observed for a rectangular hole array than that of circular holes with the same fundamental period. This difference in the amplitude transmissions in two different orientations is because of the preservation of the input linear polarization for the surface mode. When the major axis is perpendicular to the polarization of the THz beam ($E \parallel x$), it preserves the input linear polarization for the surface plasmons more than that of the $E \parallel y$ orientation.²⁰

In both orientations, the extraordinary transmission peak is found well below the cutoff frequency and may be attributed to the resonant tunneling of SPPs.^{11,12} The minima shown in Fig. 2 for both orientations can be identified as the result of Wood's anomaly observed in diffraction grating structures.²¹ Wood's anomaly minima occur when a diffracted order becomes tangent to the plane of grating. For a square lattice and normal incidence, the wavelengths of Wood's anomaly minima are approximately given by²²

$$\lambda_{\text{Wood}}^{m,n} = \frac{L}{\sqrt{m^2 + n^2}} \sqrt{\epsilon_1}. \quad (2)$$

The two calculated Wood's anomaly minima are located at 1.875 $[\pm 1, 0]$ or $[0, \pm 1]$ and 2.652 $[\pm 1, \pm 1]$ THz, respectively.

tively, for the silicon-air interface. Clearly, our observed minima in the transmission spectra are well described by Eq. (2). When the surrounding dielectric constant $\epsilon_1 \ll \epsilon_2$, the resonant wavelength for SPPs given in Eq. (1) differs very slightly from the wavelength of Wood's anomaly minima. In fact, they might partially overlap.

The observed spectral shift in the resonant frequencies with respect to the theoretical value predicted by Eq. (1) for silicon gratings was well explained.¹² In our case, instead of having half-open array structures by a dicing saw, the undercutting profile resulting from the RIE process may give rise to the discrepancy. To check the reproducibility of our measurements, the sample was flipped over and illuminated with THz pulses from the back. Transmission measurements were performed for both orientations and we have not seen any perceptible difference in either the peak position or the transmission magnitude.

The dependence of the SPP-assisted transmission properties on the dielectric constant of the surrounding materials was investigated by measuring the zero-order transmission through sandwiches made of the array and the desired materials. Four different interfaces were characterized, including air-array-air, polyethylene-array-polyethylene, quartz-array-quartz, and silicon-array-silicon. The quartz and polyethylene are fused quartz and low-density polyethylene, respectively. The surrounding silicon is moderately n doped with a resistivity of 20 Ω cm. These surrounding materials are fairly transparent to the THz frequencies and have different refractive indices of 1, 1.51, 1.98, and 3.42, respectively, for air, polyethylene, quartz, and silicon. The same subwavelength-structured sample was used as the array, and the resonance peaks in the transmission spectra were confirmed by placing the major axis of the hole perpendicular to the THz polarization ($E \parallel x$). The amplitude transmission spectra for different interfaces are shown in Fig. 3, where the $[\pm 1, 0]$ modes are represented by the dashed lines. The experimental result shows that the peak amplitude decreases when the surrounding material has a higher index and the corresponding resonance peak moves toward the lower frequency as predicted by Eq. (1). This result is also consistent with the experimental observation in the optical region.²² The observed resonant frequencies of the $[\pm 1, 0]$ mode, as a function of the surrounding refractive index, is plotted in the inset of Fig. 3.

The low-index material clearly shows pronounced maxima and minima due to the resonant excitation of SPPs and Wood's anomaly, respectively. For high-index material, however, the pronounced maxima are relatively broader because of the merging of consecutive resonance peaks. Wood's anomaly effects also appear to be weaker due to the overlapping of the resultant peaks. The resonance peak position can be resolved by increasing the periodicity of the corrugation. Residual air in between the array and the surrounding material also might contribute to distort the transmission peaks which can be solved by using the liquid as a surrounding dielectric medium. This feature enables one to tune the resonant frequency of SPPs dynamically by varying the index of refraction of the surrounding dielectric materials.

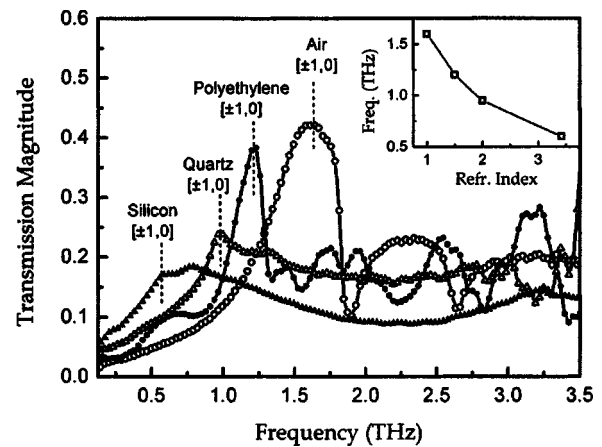


FIG. 3. Comparison of transmission spectra for different dielectric-array interfaces: Air-array-air (open circles), polyethylene-array-polyethylene (dots), quartz-array-quartz (open triangles), and silicon-array-silicon (solid triangles). The dashed lines represent $[\pm 1, 0]$ resonance peaks. The inset shows the data of the resonance frequency of the $[\pm 1, 0]$ modes as a function of the surrounding refractive index.

The authors acknowledge the stimulating discussions with Daniel Grischkowsky and John O'Hara, and the efforts of Jianming Dai. This work was partially supported by the Oklahoma EPSCoR for the National Science Foundation.

- ¹T. Ebbesen, H. Lezec, H. Ghaemi, T. Thio, and P. Wolff, *Nature (London)* **391**, 667 (1998).
- ²W. Tan, T. Preist, and R. Sambles, *Phys. Rev. B* **62**, 11 134 (2000).
- ³U. Schröter and D. Heitmann, *Phys. Rev. B* **58**, 15 419 (1998).
- ⁴J. Seidel, S. Grafström, L. Eng, and L. Bischoff, *Appl. Phys. Lett.* **82**, 1368 (2003).
- ⁵W. Barnes, A. Dereux, and T. Ebbesen, *Nature (London)* **424**, 824 (2003).
- ⁶S. Shinada, J. Hashizume, and F. Koyama, *Appl. Phys. Lett.* **83**, 836 (2003).
- ⁷D. Qu, D. Grischkowsky, and W. Zhang, *Opt. Lett.* **29**, 896 (2004).
- ⁸H. Cao and A. Nahata, *Opt. Express* **12**, 1004 (2004).
- ⁹L. Martín-Moreno, F. García-Vidal, H. Lezec, K. Pellerin, T. Thio, J. Pendry, and T. Ebbesen, *Phys. Rev. Lett.* **86**, 1114 (2001).
- ¹⁰J. Saxler, J. G. Rivas, C. Janke, H. P. M. Pellemans, P. H. Bolver, and H. Kurz, *Phys. Rev. B* **69**, 155427 (2004).
- ¹¹J. Gómez Rivas, C. Schotsch, P. Haring Bolivar, and H. Kurz, *Phys. Rev. B* **68**, 201306 (2004).
- ¹²C. Janke, J. G. Rivas, C. Schotch, L. Beckmann, P. H. Bolivar, and H. Kurz, *Phys. Rev. B* **69**, 205314 (2004).
- ¹³W. Zhang, A. Azad, and D. Grischkowsky, *Appl. Phys. Lett.* **82**, 2841 (2003).
- ¹⁴H. Ghaemi, T. Thio, D. Grupp, T. Ebbesen, and H. Lezec, *Phys. Rev. B* **58**, 6779 (1998).
- ¹⁵T. Thio, H. Ghaemi, H. Lezec, P. Wolff, and T. Ebbesen, *J. Opt. Soc. Am. B* **16**, 1743 (1999).
- ¹⁶M. A. Ordal, L. L. Long, R. J. Bell, S. E. Bell, R. R. Bell, R. W. Alexander, Jr., and C. A. Ward, *Appl. Opt.* **22**, 1099 (1983).
- ¹⁷L. Martín-Moreno, F. García-Vidal, H. Lezec, A. Degiron, and T. Ebbesen, *Phys. Rev. Lett.* **90**, 167401 (2003).
- ¹⁸M. van Exter and D. Grischkowsky, *Appl. Phys. Lett.* **56**, 1694 (1990).
- ¹⁹T.-I. Jeon and D. Grischkowsky, *Phys. Rev. Lett.* **78**, 1106 (1997).
- ²⁰R. Gordon, A. G. Brolo, A. McKinnon, A. Rajora, B. Leathem, and K. L. Kavanagh, *Phys. Rev. Lett.* **92**, 037401 (2004).
- ²¹R. W. Wood, *Phys. Rev.* **48**, 928 (1935).
- ²²T. Kim, T. Thio, T. Ebbesen, D. Grupp, and H. Lezec, *Opt. Lett.* **24**, 256 (1999).